Contents lists available at ScienceDirect

Ecological Indicators

journal homepage: www.elsevier.com/locate/ecolind

Validating the use of MODIS time series for salinity assessment over agricultural soils in California, USA

Kristen Whitney[a], Elia Scudiero[b,c,*], Hesham M. El-Askary[d,e,f], Todd H. Skaggs[c], Mohamed Allali[e], Dennis L. Corwin[c]

[a] Computational and Data Sciences Graduate Program, Schmid College of Science and Technology, Chapman University, Orange, CA 92866, USA
[b] Department of Environmental Sciences, University of California Riverside, Riverside 92521, CA, USA
[c] United States Salinity Laboratory, United States Department of Agriculture – Agricultural Research Service, Riverside 92507, CA, USA
[d] Center of Excellence in Earth Systems Modeling & Observations, Chapman University, Orange 92866, CA, USA
[e] Schmid College of Science and Technology, Chapman University, Orange 92866, CA, USA
[f] Department of Environmental Sciences, Faculty of Science, Alexandria University, Moharem Bek, Alexandria 21522, Egypt

ARTICLE INFO

Keywords:
Soil salinity indicator
Salinity stress
Vegetation reflectance
Remote sensing
MODIS time series data

ABSTRACT

Testing soil salinity assessment methodologies over different regions is important for future continental and global scale applications. A novel regional-scale soil salinity modeling approach using plant-performance metrics was proposed by Zhang et al. (2015) for farmland in the Yellow River Delta, China, a region with a humid continental/subtropical climate. The one-year integral of temporally interpolated MODIS Enhanced Vegetation Index (EVI) time series data was proposed as an explanatory variable for agricultural soil salinity modeling. Here, we test such a methodology in California's Central Valley, USA, a region with a semi-arid Mediterranean climate. Time series of EVI, Normalized Difference Vegetation Index (NDVI), and Canopy Response Salinity Index (CRSI) were created for the 2007–2013 period. Seventy-three MODIS pixels surveyed for 0–1.2-m soil salinity in 2013 were used as the ground-truth dataset. Our results validate the tested approach: the 2013 integral of CRSI (best performing index) had a Pearson correlation coefficient (r) of −0.699 with salinity. Results obtained using temporally integrated data were almost always better than those obtained using individual data. Furthermore, we show that the methodology can be improved by the use of multi-year data. Further research is needed to improve spatial resolution and the selection of vegetation indices.

1. Introduction

1.1. Soil salinity and agriculture

Elevated levels of soluble salts (e.g., Cl^-, Na^+) in soils are a major threat to irrigated and rain-fed agriculture worldwide (Ghassemi et al., 1995; Metternicht and Zinck, 2003; Ivits et al., 2011). Even when present in small amounts, soluble salts reduce yields for many crops. According to the U.S. Salinity Laboratory (US Salinity Laboratory Staff, 1954), most agricultural plants cannot grow if soil salinity exceeds 16 dS m^{-1}, where salinity is quantified as the electrical conductivity of a saturated soil paste extract (EC_e). Soils are classified as saline when $EC_e > 4$ dS m^{-1}. About 23% (ca. 0.34×10^9 ha) of worldwide farmland is estimated to be saline (ITPS: Intergovernmental Technical Panel on Soil, 2015). Knowledge and mapping of the spatial distribution of soil salinity is important for irrigation and drainage management, and for setting water and environmental policies that affect the economic sustainability of farming systems (Lambert and Southard, 1992; Letey, 2000; Welle and Mauter, 2017).

Many geological (e.g., pedogenesis), geomorphological (e.g., elevation gradients), meteorological (e.g., rainfall and evapotranspiration totals), and management (e.g., irrigation management) factors affect the salinity levels of irrigated soils (Elnaggar and Noller, 2009; Akramkhanov et al., 2011; Scudiero et al., 2014a; Vermeulen and Van Niekerk, 2017). This multiplicity of contributing factors makes it extremely difficult to extrapolate local point measurements of soil salinity to regional scales. Satellite based imagery can be used as a covariate in salinity mapping models (Wu et al. 2014) because it captures variations of salinity at different scales (e.g., subfield and between fields variations) (Scudiero et al., 2017).

Abbreviations: CRSI, canopy response salinity index; EC_e, electrical conductivity of the saturation extract (dS m^{-1}); EVI, Enhanced Vegetation Index; NDVI, Normalized Difference Vegetation Index; SG, Savitzky–Golay; VI, vegetation index; WSJV, western San Joaquin Valley; YI, yearly integral

* Corresponding author. USDA-ARS, United States Salinity Laboratory, 450 West Big Springs Rd., Riverside, CA 92507-4617, USA.
E-mail addresses: elia.scudiero@ucr.edu, elia.scudiero@ars.usda.gov (E. Scudiero).

https://doi.org/10.1016/j.ecolind.2018.05.069
Received 18 January 2018; Received in revised form 22 May 2018; Accepted 25 May 2018
1470-160X/ Published by Elsevier Ltd.

1.2. Remote sensing of soil salinity

1.2.1. Surface salinity versus root-zone salinity

Salinity at or near the soil surface (~ top 0.05–0.1 m) can be readily identified over large regions using remote sensing tools (Allbed and Kumar, 2013). However, monitoring surface salinity is of limited interest for agricultural applications. Especially in irrigated agriculture, salinity generally accumulates deeper in the soil profile. Other than during germination, crops are influenced by soil conditions over the entire root zone, which can extend down to 0.5–1.2 m and deeper depending on the crop. For example, Lobell et al. (2007) found that in the Colorado River Delta region, Mexico, soil salinity levels at 0.3–0.6 m had a higher impact on plant growth than salinity at 0–0.3 m. Determining root zone soil salinity from surface measurements is challenging: often, there is not a direct correlation between surface and root-zone soil salinity (e.g., Zare et al., 2015).

Over large regions, indirect measures of root zone soil salinity can be obtained through measurements of crop performance (e.g., greenness). Visible, near infrared, infrared, and thermal reflectance can be used as a measure of salinity stress (Lobell et al., 2010; Wu et al., 2014; Zhang et al., 2015; Ivushkin et al., 2017). However, other stressors (e.g., water deficiency, pests, and nutrient deficiency) trigger similar canopy reflectance responses (e.g., higher reflectance in the visible range and lower in the infrared). Additionally, other factors, such as phenological stage, also influence canopy reflectance (Solari et al., 2008; Tagarakis and Ketterings, 2017), thus further obscuring the relation between reflectance and salinity. Multi-temporal analysis of canopy reflectance can be used to isolate the effects of soil salinity from other confounding factors (Lobell et al., 2010; Wu et al., 2014). This is possible when average root zone salinity remains fairly stable over a short period of time – up to 5–7 years (Lobell et al., 2007; Lobell et al., 2010). Conversely, other stressors (e.g., mismanagement, pests) tend to be more transient, often varying intra-annually (Scudiero et al., 2014b).

1.2.2. Detecting soil salinity with MODIS time series vegetation index data

In the last ten years, multi-temporal remote sensing data, especially visible and near-infrared reflectance, has been used in several studies to detect soil salinity (Lobell et al., 2007; Platonov et al., 2013; Wu et al., 2014; Scudiero et al., 2016b, Gorji et al., 2017). One of the most noteworthy studies was done by Zhang et al. (2015). They used Moderate Resolution Imaging Spectroradiometer (MODIS, The National Aeronautics and Space Administration – NASA, USA) time series vegetation index (VI) data. They proposed that salinity estimates from VI time-series could be improved by simulating the inter-annual VI variations through a temporal interpolation procedure. By doing so, information on crop physiology (such as seasonal integrals of VI values) can be extracted from the time series datasets and used as explanatory variables in salinity assessment models. Zhang et al. (2015) developed their methodology using ground data from the Yellow River Delta in the Dongying District, China, which encompasses a mix of humid continental and humid subtropical climates with dry winters and rainy summers, with yearly average rainfall of 600 mm (Zhang et al., 2011; Zhang et al., 2015). They reported that soil salinity correlated more strongly with integrals of VI time series (from a single growing season) than with VI from single dates. The VIs used by Zhang et al. (2015) were the Normalized Difference Vegetation Index, NDVI shown in Eq. (1) (Rouse et al., 1973):

$$\mathrm{NDVI} = \frac{(\mathrm{NIR}-\mathrm{R})}{(\mathrm{NIR}+\mathrm{R})} \quad (1)$$

where R and NIR are MODIS's red (620–670 nm) and near-infrared (841–875 nm) bands, respectively; and the Enhanced Vegetation Index, EVI shown in Eq. (2) (Huete et al., 2002):

$$\mathrm{EVI} = g \times \frac{(\mathrm{NIR}-\mathrm{R})}{(\mathrm{NIR}+c_1 \times R - c_2 \times \mathrm{B} + l)} \quad (2)$$

where B is MODIS's blue (459–479 nm) band and g, c_1, c_2, and l are aerosol and soil correcting parameters set to 2.5, 6, 7.5, and 1 respectively. They found that the one-growing-season time series integral of EVI was more strongly correlated with soil salinity and more sensitive to salinity changes than the integral of NDVI was.

1.2.3. Justification for this research

The research of Zhang et al. (2015) and other previously published regional scale salinity assessment research has been carried out over areas with fairly homogeneous meteorology (e.g., rainfall, temperature) and geomorphology (e.g., pedogenesis). Future research efforts should focus on creating national and global inventories of agricultural soil salinity (Scudiero et al., 2016a). Mapping salinity at such broad scales would entail using remote sensing over diverse geographical regions. As a step towards that goal, the current remote sensing approaches, such that proposed by Zhang et al. (2015), should be tested and validated over different geographical regions of the world.

1.2.4. Research objectives

In this study, we test the MODIS VI time-series approach proposed by Zhang et al. (2015). We evaluate the approach using a ground-truth soil salinity dataset from the western San Joaquin Valley, California, USA (Scudiero et al., 2014a), a region very different from the Yellow River Delta. Besides testing the approach of Zhang et al. (2015), we also address the following questions:

1. Should the integral value of the MODIS VI time series proposed by Zhang et al. (2015) be preferred to a seasonal average of the VIs?
2. Should multiple-year time series of MODIS VIs data be used to map salinity over semi-arid farmland, such as in California's western San Joaquin Valley, rather than single-season time series? A single year of data might not be sufficient to isolate the effect of salinity on crop metrics. In a given year, crop performance may be limited by other factors besides salinity. In that case, a multi-year analysis may be required.
3. Does MODIS EVI provide better relationships with salinity in semi-arid farmland than NDVI, as observed for continental and subtropical climates by other authors, including Zhang et al. (2015)?
4. Are there relevant scale-related limitations for the use of MODIS VIs over areas with fairly heterogeneous cropping and land use patterns, such as California's western San Joaquin Valley?

2. Materials and methods

2.1. Study area

The farmland of California's western San Joaquin Valley (WSJV, Fig. 1a) is among the most salt-affected in California (Backlund and Hoppes, 1984; Lambert and Southard, 1992). The WSJV has hot and dry summers and cool winters. Annual rainfall averages around 150–200 mm. For WSJV, the 2011 National Land Cover Database classified 0.83×10^6ha as farmland (Fry et al., 2011). According to the CropScape database (Han et al., 2012), 16.2% of WSJV farmland was cropped with orchards in 2013 (e.g., *Pistacia vera* L., *Prunus dulcis* Mill.). The rest was used for herbaceous/annual (e.g., *Solanum lycopersicum* L., *Triticum aestivum* L.) crop production (75%), for pastureland (3.3%), or left fallow (21.6%). During the 2011–2015 California drought (Williams et al., 2015), the portion of fallow land increased steadily, from 11.8% pre 2011 to 33.7% in 2015 (Scudiero et al., 2017), mostly at the expense of herbaceous crop production (Howitt et al., 2014). Farmers' decisions on land fallowing were mainly driven by surface and well-water availability and by expected revenues (Howitt et al., 2014). Scudiero et al. (2017) reported that 55% of the farmland in WSJV (excluding orchards – which were not included in theirs study) is moderately to extremely affected by soil salinity.

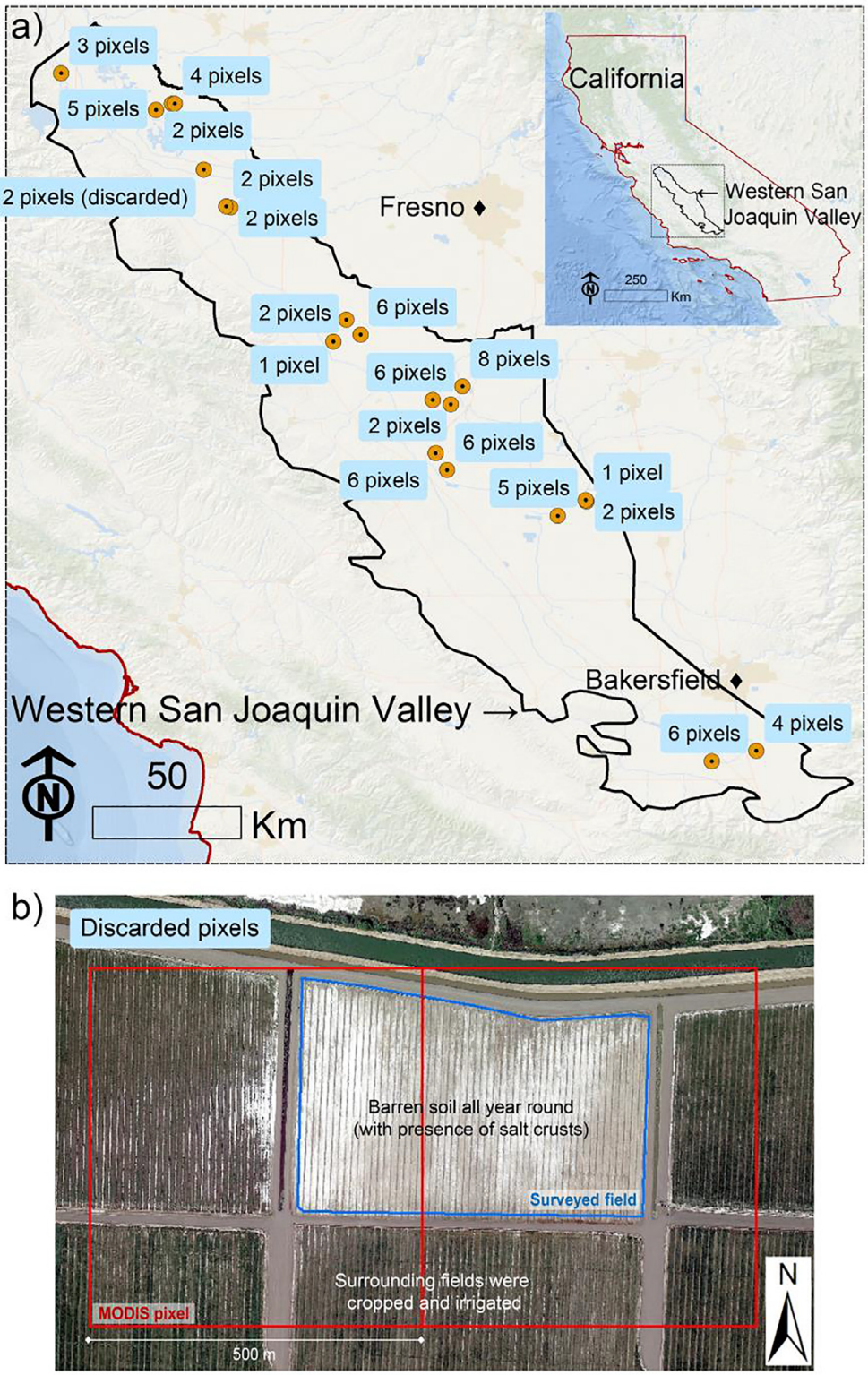

Fig. 1. a) Western San Joaquin Valley, California, USA, and the locations of the 73 MODIS pixels co-located with the ground-truth dataset, and b) the two pixels that were not used in this study.

2.2. Satellite data

2.2.1. MODIS data processing

The MODIS data were obtained from the U.S. Geological Survey through the Earth Explorer tool (https://earthexplorer.usgs.gov/). In this study, we used the same MODIS data product used by Zhang et al. (2015): the 500-m MOD09A1 Version 6 (Vermote, 2015) surface reflectance data.

The reflectance data is corrected for gaseous, aerosol, and Rayleigh scattering. MOD09A1 scenes are available as 8-day composite data. All available scenes from January 1, 2007 to December 31, 2013 were downloaded, totaling 322 8-day composite scenes. For each pixel in a

tile, MOD09A1data includes the value with the best quality from all the MODIS acquisitions within the 8-day composite period (Vermote, 2015). Surface reflectance for the blue (459–479 nm), green (454–565 nm), red (620–670 nm), and near infrared (841–875 nm) spectral bands were used. The MOD09A1 Quality control layer was used to remove data characterized by excessive atmospheric disturbance. Following the directions of Zhang et al. (2015) and Xiao et al. (2005), pixels with a blue reflectance greater than 20% were marked as cloudy pixels and, consequently, removed.

The surface reflectance data was used to calculate VIs for each 8-day composite MOD09A1 scene. As done by Zhang et al. (2015), we calculated NDVI and EVI. Additionally we also calculated the Canopy Response Salinity Index (CRSI) as shown in Eq. (3) (Scudiero et al., 2014a):

$$CRSI = \sqrt{\frac{(NIR \times R) - (G \times B)}{(NIR \times R) + (G \times B)}} \quad (3)$$

where G is the green band. The CRSI was used because of its good performance for soil salinity assessment using Landsat 7 reflectance in the WSJV (Scudiero et al., 2014a).

2.2.2. Vegetation indices time series smoothing

Following Zhang et al. (2015), daily values of CRSI, NDVI, and EVI were calculated by applying a Savitzky–Golay (SG) filter (Savitzky and Golay, 1964) to the 8-day composite VI values. With an SG filter, a moving-window polynomial least-squares fit is used to smooth temporal data, reduce noise, and produce daily values (Jönsson and Eklundh, 2004). A larger window size results in smoother curves at the expense of flattening local peaks (Jönsson and Eklundh, 2004; Kim et al., 2014). Jönsson and Eklundh (2004) provide a full explanation of the SG filter. Zhang et al. (2015) used a second degree polynomial fit and window size of 8. We used MATLAB R2017a (The MathWorks, Inc., Natick, Massachusetts, USA) to apply the SG filter with a second degree polynomial and a window size of 5 (i.e., 32 days). The smaller window size was selected to increase the time series resolution over local peak values of the VIs.

The smoothed time series were used to calculate yearly integral (YI) values for each VI. We tested the use of the 2013 YI for salinity assessment. We also tested the multi-year maximum YI value over consecutive years prior to 2013, going back to 2007. For example, the 3-year maximum YI equates to, at each pixel, the maximum YI value for the years 2011, 2012, and 2013.

2.3. Ground-truth data

The USDA-ARS WSJV soil salinity dataset (Scudiero et al. 2014a) was used as the ground-truth dataset in this research. The dataset comprises 41,779 EC_e data points for the 0–1.2-m soil profile. The dataset was collected over 22 fields, totaling 542 ha. The dataset was compiled using a combination of 41,779 electromagnetic induction readings and 267 soil salinity measurements made on composite 0–1.2-m soil cores. The laboratory salinity data were used to calibrate the electromagnetic induction measurements using field-by-field linear regression modeling, with an overall coefficient of determination of $R^2 = 0.93$ (Scudiero et al., 2014a).

We interpolated the 41,779 EC_e data points onto the 500 × 500 m MODIS grid using simple kriging, following the directives of Lobell et al. (2010). Isotropic exponential semivariograms were used in the kriging models. The spatial interpolations were made with ArcMap 10.1 (ESRI, Redlands, California, USA) resulting in 75, 500 × 500 m, EC_e ground-truth estimates (Fig. 1a). The agricultural fields in the dataset did not align with the MODIS grid. Therefore each of the 75 ground-truth measurements had different degrees of pixel coverage, which we recorded. For example, 50% coverage indicates that salinity was measured over half of the MODIS pixel area. Of the 75 ground-truth cells, two were discarded from the analysis because of heterogeneous and contrasting land use (Fig. 1b). The remaining 73 were retained for further analyses and were classified as cropped or fallow on a year-to-year basis according to the CropScape database (Han et al., 2012). MODIS pixels were classified as cropped or fallow based on the most frequent CropScape land use classification (at 30 × 30 m) occurring within an overlaying MODIS pixel.

2.4. Statistical analyses

Pearson correlation analyses were carried out between soil salinity and remote sensing data. Additionally, weighted regressions were developed between the remote sensing data (independent variable) and soil salinity (explanatory variable) for data in each land use class (i.e., cropped and fallow pixels). Weighted least squares regression was carried out using the *lm*() function from the *stats* package in R 3.4.1 (R Core Team, 2017), using pixel coverage as the weight.

3. Results and discussion

3.1. Soil salinity measurements

At the ground-truth sites, soil salinity for the 0–1.2 m soil profile ranged between 0.01 and 18.31 dS m^{-1}, with a median of 5.17 dS m^{-1}. Within each pixel, surveyed farmland coverage ranged between 0.23 and 96.45%. Additional statistics for EC_e and pixel coverage are reported in Table 1.

In 2013, when the soil salinity surveys were carried out, 46 pixels were cropped and 27 were fallow (See Table 2 for land use information, 2007 through 2012). Through 2007–2013, 37 of the cropped pixels were cropped every year, whereas 9 of the fallow pixels were fallow every year. Because of the shifting cropping patterns in WSJV, updated datasets identifying crop type at the field scale (e.g., Han et al., 2012; Zhu et al., 2017) are of great value for properly classifying and analyzing pixels.

3.2. MODIS pixel size

A MODIS pixel covers 25 ha. The ground truth survey fields ranged between 2.3 and 63.0 ha, with an average size of 24.1 ha. Salinity ground truth information within each pixel was not homogeneous. The average within-pixel salinity variance was 2.54 $dS^2 m^{-2}$. Thus upscaling the ground-truth measurements to the 500 × 500-m MODIS resolution resulted in a loss of information. This was not surprising since previous studies have shown that soil salinity in WSJV often exhibits high variability over short distances (Lesch et al., 1992). The loss of information due to the coarse resolution suggests that the MODIS pixel size may be too large to map soil salinity at the sub-field scale in WSJV. Scudiero et al. (2016b) assessed WSJV salinity using Landsat 7 imagery with a 30 × 30 m resolution, whereas Scudiero et al. (2017) found that the optimal resolution was around 20 × 20 m when evaluating EVI and soil salinity at resolutions ranging from 2 × 2 to 100 × 100 m.

Table 1
Salinity (EC_e) for the 0–1.2 m soil profile and pixel coverage for the 73 ground-truth locations.

	EC_e (dS m^{-1})	Pixel coverage (%)
Minimum	0.01	0.23
Maximum	18.31	96.45
Average	6.81	30.07
Median	5.17	24.10
Standard Deviation	4.98	26.88
Skewness	0.69	0.85
Kurtosis	−0.80	−0.29

Table 2
Number of pixels classified as cropped or fallow in all considered years.

Land use	Year						
	2007	2008	2009	2010	2011	2012	2013
Cropped	55	49	43	41	49	59	46
Fallow	18	24	30	32	24	14	27

Much of WSJV is also characterized by short-scale variations in land use. This is evident when examining various imagery and databases (e.g., the National Aerial Imagery Program of the U.S. Department of Agriculture, Google Earth, and the U.S. Land Use National Land Cover Database). Most farm-fields in WSJV are next to paved and unpaved roadways, railways, surface water bodies (e.g., drainage canals), urban, and industrial land. Non-agricultural lands have different reflectance properties than cropped fields (Chen et al., 2005). At the MODIS resolution, narrow non-agricultural features cannot be discriminated from farmland (Gao et al., 2006), making it hard to monitor agricultural processes.

Zhang et al. (2015) discussed similar limitations related to the MODIS resolution when developing the remote sensing methodology in the Yellow River Delta. Nevertheless, their methodology works best when remote sensing data are available at high temporal resolution, such as with MODIS. Moreover, despite all within-pixel noise sources, MODIS-based estimates may be able to characterize local (e.g., farm-scale) average response, as shown in evapotranspiration modeling studies (McCabe and Wood, 2006). Accurate salinity information at such resolution would still be very valuable for natural resource management (Welle and Mauter, 2017).

3.3. Vegetation indices time-series

Fig. 2 shows the Pearson correlation coefficient (r) between soil salinity and all unfiltered 8-day composite scenes for all VIs in 2013. Pearson's r ranged between -0.715 and -0.335 for CRSI, between -0.581 and -0.233 for NDVI, and between -0.547 and -0.150 for EVI. In 2013, for all VIs, the weakest r values were observed in the months of January through May, whereas stronger r values were observed from late July through early December. For comparison, Ivushkin et al. (2017) observed strongest correlations between thermal imagery and soil salinity over cotton (*Gossypium hirsutum* L.) through late July and mid-August in the farmland of Uzbekistan's Syrdarya Province. The temporal variation in the correlation indicates that an arbitrary single date should not be used to map soil salinity through canopy reflectance, as also discussed by Lobell et al. (2010) and Zhang et al. (2015). Variability in the plant reflectance – salinity relationship through the year may be due to: *i*) changing plant response to salt stress at different vegetation stages (Maas et al., 1986; Baath et al., 2017), *ii*) the influence of other stressors (e.g., water stress, pests) (Lobell et al., 2010), and/or *iii*) the fact that, even when unstressed, crop reflectance is influenced by species × growth-stage × soil background interactions (Gausman and Allen, 1973; Huete et al., 1985; Li et al., 2001).

The unfiltered 8-day composite VI values were temporally interpolated using the SG filter. Fig. 3 shows an example application of the filter to NDVI data at a selected location. Daily values of CRSI, NDVI, and EVI were obtained from the filtered time series. Zhang et al. (2015) used the time series to calculate integral values for EVI and NDVI during the crop-growing season only. Lobell et al. (2010) also used only data from the crop growing season. The WSJV growing season is nearly year round. Therefore, we did not discard any data from the VI time series. Yearly integrals (YI) of the time series of all three indices were then calculated at each pixel.

The 2013 YI correlations with soil salinity were $r = -0.699$ (CRSI), $r = -0.644$ (NDVI), and $r = -0.602$ (EVI). These r values are reported in Fig. 2 (dotted lines). For CRSI, most (95.7%) of the r yielded by single unfiltered 8-day composite scenes were smaller than that yielded when the YI was used. For NDVI and EVI, no single unfiltered 8-day composite scene had stronger r than the respective YI. The YI values yielded slightly stronger correlation coefficients than those between salinity and the yearly average of the unfiltered 8-day composite scenes (Fig. 2, solid lines).

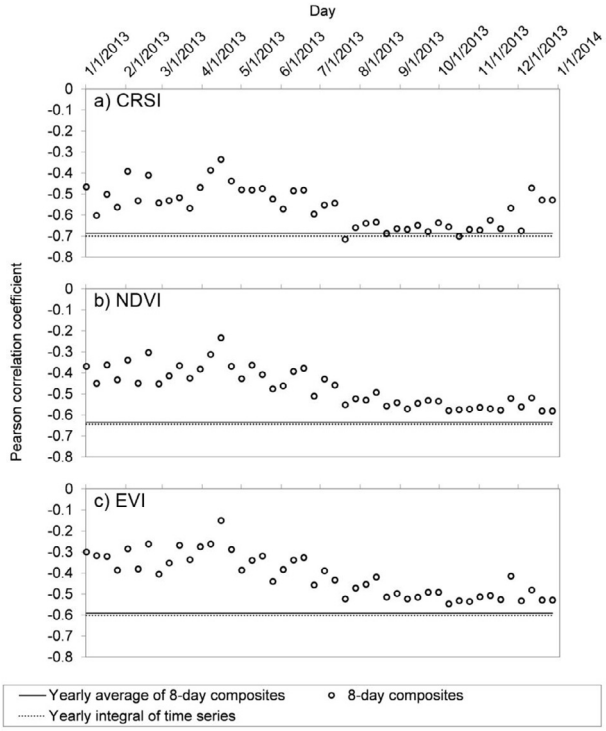

Fig. 2. Pearson correlation coefficients for soil salinity vs. each 8-day composite scene in 2013 (circles), their yearly average (solid line), and the integral of the vegetation index time series (dotted line), for a) canopy response salinity index (CRSI), b) normalized difference vegetation index (NDVI), and c) enhanced vegetation index (EVI).

These correlation results presented in Fig. 2 indicate that the methodology proposed by Zhang et al. (2015) is an effective means for assessing root-zone soil salinity at different geographical regions besides the Yellow River Delta. The Zhang et al. (2015) methodology is a potential candidate for soil salinity assessment over regions having differing climates and farming systems. It is important to notice, however, that similar multi-year remote sensing analyses can be used to characterize the spatial variability of permanent stressors other than salinity, such as heavy metals in the root zone (Liu et al., 2018).

3.4. Detecting soil salinity with multi-year MODIS time series

Single-year or single-growing-season VI integrals provide intra-annual information on crop status (Zhang et al., 2015). In Table 3, we show r for the relationships between salinity and *i*) the 2013 YI and *ii*) and the multi-year maxima of the YI between 2013 and consecutive previous years, back to 2007. The strength of the relationship between remote sensing data and salinity was greater when multi-year maxima were used.

In Table 3, r values are reported for the full dataset (73 pixels) and for sub-datasets having different pixel-coverage lower limits. Note that r values for different sub-datasets (different pixel coverage classes) should not be compared directly because they all have different sample size, average, and variance. The different r values within each row in Table 3 should be compared instead. To aid the comparison, we provide a color scale indicating the rank of the r coefficient in each row: the

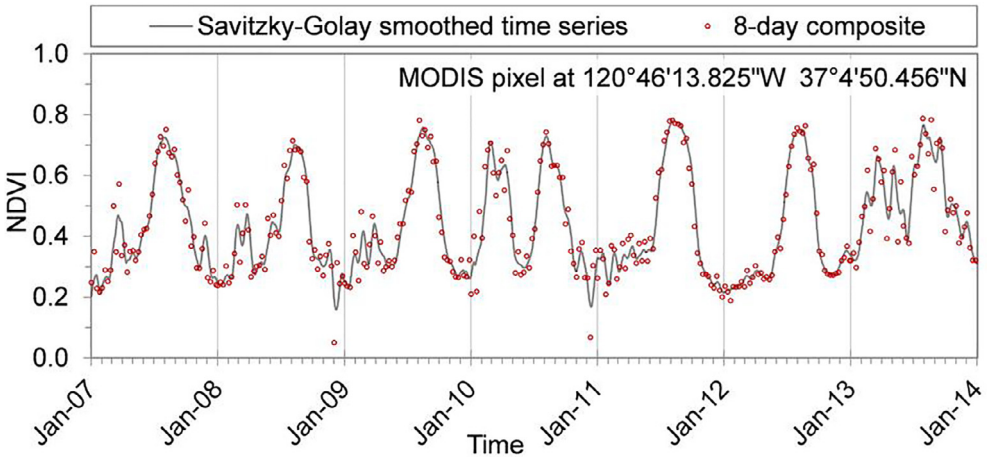

Fig. 3. Example of a Savitzky–Golay smoothed time series for MODIS normalized difference vegetation index (NDVI) for a selected pixel from January 1st 2013 to December 31st 2013.

darker the cell, the stronger the relationship between salinity and the selected YI combination. In the vast majority of the considered sub-datasets, the remote sensing – salinity relationship was stronger when multiyear maximum YIs of VI were used.

These results are consistent with previous research (Lobell et al., 2007; Lobell et al., 2010; Wu et al., 2014; Scudiero et al., 2014b). In particular, Scudiero et al. (2014b) showed that VIs in saline areas of a maize field in Northeastern Italy had low annual variation, which is consistent with the findings of Zhang et al. (2015). However, Scudiero et al. (2014b) showed that areas under water stress were also characterized by low annual VI variability. Only when using multiple-year VI data could they differentiate between salinity and water stress. Moreover, using multi-year maxima data allows associating the canopy reflectance data to other time-specific environmental covariates (crop type, meteorology). The use of such covariates is known to be very useful for salinity mapping models (Lobell et al., 2010; Scudiero et al., 2016b).

Previous studies used four (Platonov et al., 2013; Wu et al., 2014) to seven (Lobell et al., 2007; Lobell et al., 2010; Scudiero et al., 2016b) years of remote sensing data to map soil salinity. On the dataset used here, the strongest correlations with salinity were obtained when 2 years of VI data were used. Apparently, the optimal time span cannot be specified a priori. A tradeoff must be considered when selecting the size of the multi-year window: wider time spans allow reducing the influences of confounding factors (e.g., local transient stressors) in the crop reflectance – soil salinity relationship; yet, the wider the time window the higher the chance that sizeable changes in root-zone average salinity may happen. Several combinations of multi-year data should be tested to select the best explanatory variable for the desired salinity assessment model.

The strength of the correlations in Table 3 was generally ordered as CRSI > NDVI > EVI. Scudiero et al. (2014a) observed the same hierarchy for these indices when calculated from Landsat 7 data. Conversely, Lobell et al. (2010) and Zhang et al. (2015) indicated that MODIS EVI outperformed MODIS NDVI for soil salinity assessment in their study areas. The quality of reflectance information for vegetation indices changes according to spatial location because of atmospheric disturbance and other factors influencing satellite multispectral measurements (Hadjimitsis et al., 2010; Pettorelli et al., 2005). In areas characterized by rainy summers, such as China's Yellow River Delta, NDVI might not perform as well as EVI because of atmospheric disturbance when vegetation is at its maximum growth for the year. Conversely, clouds and aerosols may not be as relevant in the WSJV because of different meteorology. This indicates that preliminary analyses to select the best VI should always be carried out locally, as proposed by Scudiero et al. (2014a) and Zhang et al. (2015). It is always important to keep in mind that VIs are not stress-specific: multi spectral canopy reflectance should be interpreted as a relative indication of crop status.

As indicated by Lobell et al. (2010) and Zhang et al. (2015), cropped and fallow farmland have different reflectance characteristics over time. The yearly time series of the 2-year maximum YIs datasets are shown in Fig. 4, for the two land use types. The figure depicts the median and the 25th-75th percentile intervals. Out of the 73 pixels, 57 were cropped in Fig. 4a (CRSI), 54 in Fig. 4b (NDVI), and 55 in Fig. 4c (EVI). The median salinities were 4.8 (CRSI, Fig. 4a), 4.6 (NDVI, Fig. 4b), and 4.7 (EVI, Fig. 4c) dS m^{-1} over the cropped pixels, and 8.1 (CRSI, Fig. 4a), 12.0 (NDVI, Fig. 4b), and 10.9 (EVI, Fig. 4c) dS m^{-1} over the fallow pixels. Yearly integrals for the median time series were equal to 296.0 (cropped) and 276.6 (fallow) for CRSI, 139.8 (cropped) and 88.6 (fallow) for NDVI, and 81.2 (cropped) and 52.5 (fallow) for EVI. For all VIs, the index values peaked around the beginning of April for both cropped and fallow pixels. Cropped pixels exhibited a second peak during the summer months, whereas the fallow pixels steadily decreased during summer and fall. It is evident that, in the WSJV, the two land uses generate disparate VI behavior during the year. They should, therefore, be analyzed separately in remote sensing salinity assessment models, as proposed by Lobell et al. (2010) and Zhang et al. (2015).

The 2-year maximum YIs were regressed against soil salinity for cropped and fallow pixels separately. The results for all three VIs are reported for cropped pixels in Table 4 and for fallow pixels in Table 5. Fig. 5 shows results for CRSI only. As proposed by Zhang et al. (2015), we fit the data over cropped pixels with simple linear regressions, whereas fallow pixel data were fit with quadratic models. Pixel coverage was used to weight the data in the ordinary least squares regressions. For comparison, unweighted regressions are also reported in Tables 4 and 5. The regressions were all highly significant (p-values < 0.01), and a large portion of the variance in the remote sensing data was explained by variations in the soil salinity dataset. In particular, the joint use of regression equations [R1] (Table 4) and [R7] (Table 5) explained 67.8% of the total variance of the 2-year maximum YI for CRSI, Eqs. [R3] and [R9] explained 63.7% of the total variance for NDVI, and Eqs. [R5] and [R11] explained 51.0% of the total variance for EVI.

In general, the response of crops to soil salinity follows the Maas and Hoffman two-piece response curve (Maas and Hoffman, 1977): below a crop-specific threshold salinity value, crops are not affected by salinity; above the threshold value, crop performance (e.g., yield) decreases linearly according to a crop-specific slope. Thus, salinity predictions using CRSI (Fig. 5) and other VIs at low salinity ranges where crops are

Table 3
Person correlation coefficients for soil salinity (EC_e) with yearly integrals of MODIS canopy response salinity index (CRSI, top), normalized difference vegetation index (NDVI, center), and enhanced vegetation index (EVI, bottom) calculated from the Savitzky–Golay smoothed time series. Correlation coefficients shown for the Savitzky–Golay yearly integrals of 2013 and the yearly maxima (Max) between 2013 and consecutive previous years (back to 2007). Correlation coefficients are shown for the full dataset and for sub datasets having decreasing ground-truth pixel coverage. For each sub dataset, increasing intensity of blue indicates increasing strength of Pearson correlation coefficient.

	Savitzky–Golay CRSI - yearly integral							Average of observed EC_e (dS m^{-1})	Variance of observed EC_e (dS^2 m^{-2})
Pixel coverage (n)	2013	2-yr Max	3-yr Max	4-yr Max	5-yr Max	6-yr Max	7-yr Max		
Full dataset (73)	-0.699	-0.729	-0.523	-0.483	-0.483	-0.476	-0.458	6.8	26.9
≥ 15% (44)	-0.732	-0.804	-0.588	-0.591	-0.591	-0.567	-0.563	7.1	20.8
≥ 30% (30)	-0.763	-0.860	-0.653	-0.655	-0.655	-0.688	-0.671	7.5	23.5
≥ 45% (20)	-0.808	-0.840	-0.732	-0.723	-0.723	-0.772	-0.757	7.7	26.0
≥ 60% (12)	-0.773	-0.869	-0.745	-0.722	-0.722	-0.761	-0.755	7.9	29.5
≥ 75% (7)	-0.841	-0.900	-0.754	-0.720	-0.720	-0.793	-0.775	7.4	37.0
	Savitzky–Golay NDVI - yearly integral								
Full dataset (73)	-0.644	-0.692	-0.618	-0.588	-0.589	-0.578	-0.541	6.8	26.9
≥ 15% (44)	-0.664	-0.758	-0.615	-0.627	-0.631	-0.610	-0.570	7.1	20.8
≥ 30% (30)	-0.644	-0.748	-0.596	-0.616	-0.626	-0.628	-0.586	7.5	23.5
≥ 45% (20)	-0.715	-0.697	-0.618	-0.626	-0.633	-0.641	-0.600	7.7	26.0
≥ 60% (12)	-0.638	-0.705	-0.598	-0.600	-0.602	-0.587	-0.534	7.9	29.5
≥ 75% (7)	-0.653	-0.721	-0.667	-0.645	-0.653	-0.643	-0.584	7.4	37.0
	Savitzky–Golay EVI - yearly integral								
Full dataset (73)	-0.602	-0.629	-0.570	-0.480	-0.486	-0.493	-0.468	6.8	26.9
≥ 15% (44)	-0.624	-0.698	-0.565	-0.530	-0.560	-0.567	-0.546	7.1	20.8
≥ 30% (30)	-0.612	-0.701	-0.580	-0.569	-0.604	-0.615	-0.594	7.5	23.5
≥ 45% (20)	-0.675	-0.635	-0.572	-0.548	-0.600	-0.626	-0.603	7.7	26.0
≥ 60% (12)	-0.611	-0.664	-0.621	-0.598	-0.643	-0.620	-0.585	7.9	29.5
≥ 75% (7)	-0.634	-0.688	-0.687	-0.657	-0.713	-0.700	-0.663	7.4	37.0

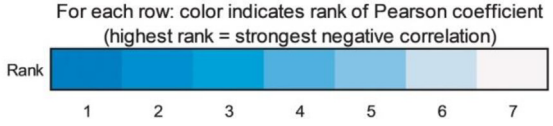

not stressed are expected to have low accuracy (Scudiero et al., 2016b).

The halophytes that generally dominate fallow farmland grow best on soils with moderately high to high salinity (around $8 < EC_e < 12$ dS m^{-1}), rather than non-saline soils (BOSTID: Board on Science and Technology for International Development, 1990; Zhang et al., 2011). Low VI YIs (e.g., Fig. 5) may correspond, therefore, to fallow soils having low or high salinity, as also observed by Zhang et al. (2015). The use of canopy reflectance alone is therefore not advised for salinity assessment over fallow land because it cannot reliably differentiate very low and very high salinities.

During the two years under consideration (2012 and 2013), the whole WSJV was under a historical drought (Williams et al., 2015). Drought was not expected to affect plant growth on irrigated cropped pixels. Conversely, vegetation growth at the non-irrigated fallow pixels may have been reduced by drought, possibly reducing the accuracy of the regressions in Table 5.

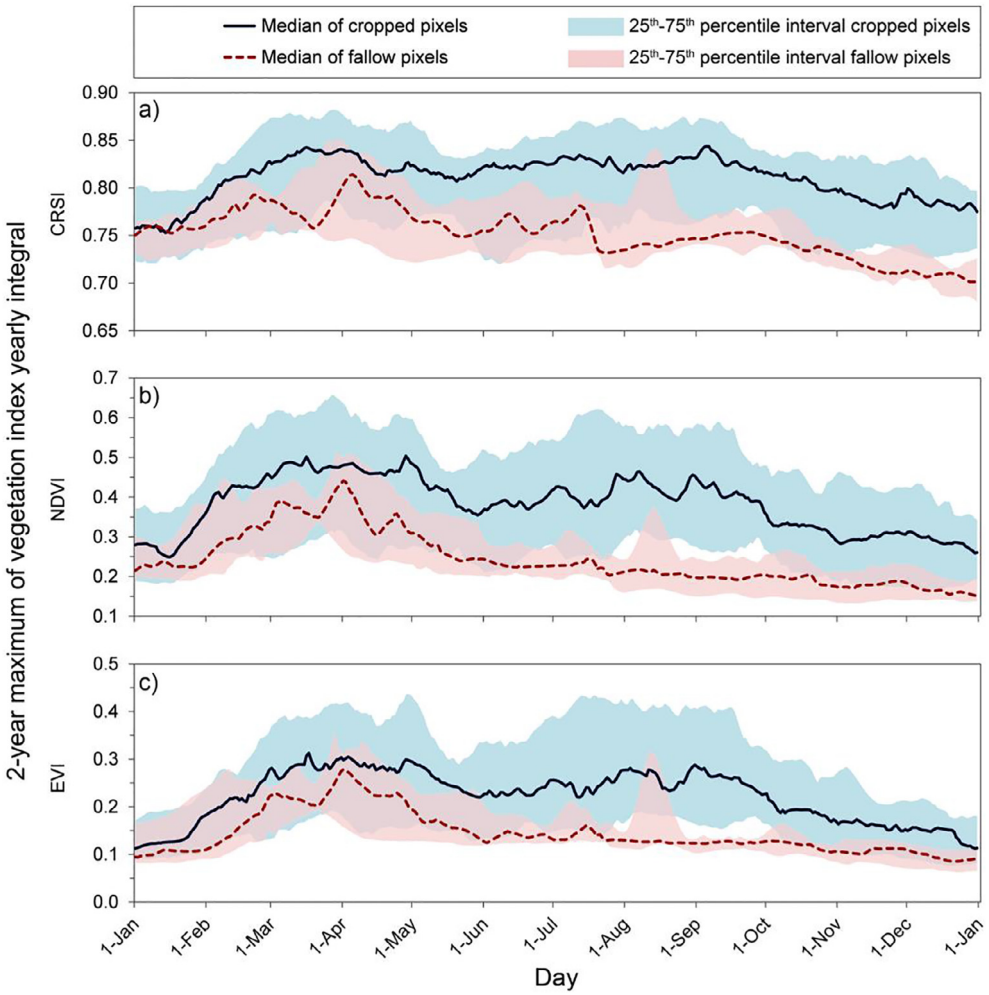

Fig. 4. Median yearly time series for the 2-year maxima of the vegetation index time series for cropped (solid blue line) and fallow (dashed red line) pixels. The 25th-75th percentile intervals are shown in blue for cropped (background) and fallow (forefront) pixels. Vegetation indices are: a) Canopy Response Salinity Index (CRSI), b) Normalized Difference Vegetation Index (NDVI), and c) Enhanced Vegetation Index (EVI). Please notice that the vertical axes have different scales for each vegetation index.

4. Conclusions

Testing soil salinity assessment methods over different regions is important for future development of continental and global scale maps and models. In this paper we tested, validated, and improved a data preprocessing methodology proposed by Zhang et al. (2015) that can be used to improve the strength between remote sensing data and soil salinity. We conclude that:

1. Temporal interpolation of the vegetation index (VI) time series, using the Savitzky–Golay filter, provided stronger correlations with salinity than unfiltered VI data;
2. Multi-year remote sensing datasets provided stronger correlations with soil salinity than single-year data. In particular, correlations between VIs and soil salinity were much stronger with a multi-year maximum approach that included separating data by land use type. The Zhang et al. (2015) methodology, when used with a multi-year maximum approach, was particularly effective when used over farmland cropped with herbaceous plants (e.g., maize, cotton, alfalfa). Over fallow land, the quadratic relationship between salinity and canopy reflectance make remote sensing data harder to interpret: lower multi-year maxima of VI integrals could be due to either

Table 4
Weighted and unweighted linear regressions between the 2-year maxima of the vegetation index yearly integrals and soil salinity for cropped pixels. Vegetation indices are: Canopy Response Salinity Index (CRSI), Normalized Difference Vegetation Index (NDVI), and Enhanced Vegetation Index (EVI).

INDEX	N	Type	Slope			Intercept			R^2	p-value	Equation ID
			Value	St.Err.	Pr(> |t|)	Value	St.Err.	Pr(> |t|)			
CRSI	57	Weighted	−3.45	0.303	< 0.001	312.66	2.26	< 0.001	0.702	< 0.001	[R1]
		Unweighted	−3.51	0.285	< 0.001	312.39	2.25	< 0.001	0.734	< 0.001	[R2]
NDVI	54	Weighted	−7.44	0.955	< 0.001	181.41	7.04	< 0.001	0.538	< 0.001	[R3]
		Unweighted	−7.88	0.957	< 0.001	184.95	6.61	< 0.001	0.566	< 0.001	[R4]
EVI	55	Weighted	−5.06	0.760	< 0.001	117.32	5.69	< 0.001	0.455	< 0.001	[R5]
		Unweighted	−5.10	0.764	< 0.001	117.14	5.38	< 0.001	0.457	< 0.001	[R6]

Table 5
Weighted and unweighted quadratic regressions between the 2-year maxima of the vegetation index yearly integrals and soil salinity for fallow pixels. Vegetation indices are: Canopy Response Salinity Index (CRSI), Normalized Difference Vegetation Index (NDVI), and Enhanced Vegetation Index (EVI).

INDEX	N	Type	Quadratic coefficient			Intercept			R^2	p-value	Equation ID
			Value	St.Err.	Pr(> |t|)	Value	St.Err.	Pr(> |t|)			
CRSI	16	Weighted	−0.08	0.021	0.003	287.78	3.54	< 0.001	0.471	0.003	[R7]
		Unweighted	−0.03	0.024	n.s.	280.69	68.58	< 0.001	0.124	n.s.	[R8]
NDVI	19	Weighted	−0.10	0.025	0.001	109.93	4.11	< 0.001	0.474	0.001	[R9]
		Unweighted	−0.06	0.032	n.s.	106.56	5.55	< 0.001	0.188	n.s.	[R10]
EVI	18	Weighted	−0.07	0.018	0.002	68.49	3.05	< 0.001	0.477	0.002	[R11]
		Unweighted	−0.05	0.029	n.s.	67.65	5.03	< 0.001	0.160	n.s.	[R12]

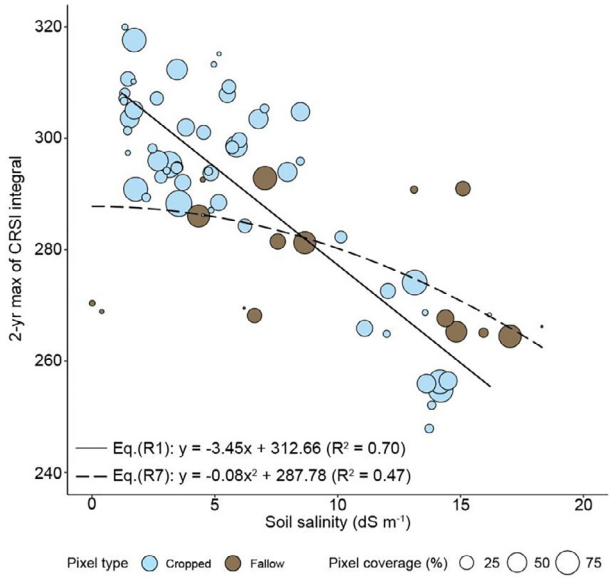

Fig. 5. Relationship between the 2-year maximum (max) of the annual integral of MODIS Canopy Response Vegetation Index (CRSI) and soil salinity.

very low or very high soil salinity;

3. We observed that the strength of the correlations coefficients between VIs and salinity were generally ordered as CRSI > NDVI > EVI. Our results, when compared to those of Zhang et al. (2015), indicate that VI applicability is region specific. Zhang et al. (2015) as well as other authors indicated that better performances were to be expected when using MODIS EVI, rather than MODIS NDVI, for salinity assessment. We observed the opposite. The difference may be due to environmental differences between the region where Zhang et al. (2015) developed their study (Yellow River Delta, China) and our study area (California's western San Joaquin Valley). We advise preliminary testing to identify the VI performing best at any region of interest;
4. The spatial resolution of MODIS is not ideal for salinity assessment over California farmland, and other land with similar short-scale variations of soil salinity, agronomic practices, and land use (e.g., small-sized fields surrounded by water canals and roads). Higher resolution remote sensing data is needed to address these issues. Future work should focus on the use of high spatial and temporal resolution satellites, such as those in the Sentinel program, operated by the European Space Agency. Moreover, the use of thermal imagery, which was not evaluated in this study, should be considered as complementary to the visible and near-infrared reflectance data, as proposed by other authors, including Wu et al. (2014) and Ivushkin et al. (2017).

Further validation of the method should be carried out over different regions, with different environments and agronomic practices (e.g., rainfed agriculture), before accurate continental and global soil salinity assessment models can be developed.

Acknowledgement

Thanks to Dr. Ray G. Anderson for help and advice on the pre-processing and quality screening of the MODIS data.

References

Akramkhanov, A., Martius, C., Park, S., Hendrickx, J., 2011. Environmental factors of spatial distribution of soil salinity on flat irrigated terrain. Geoderma 163 (1–2), 55–62. http://dx.doi.org/10.1016/j.geoderma.2011.04.001.

Allbed, A., Kumar, L., 2013. Soil salinity mapping and monitoring in arid and semi-arid regions using remote sensing technology: a review. Adv Remote Sens. 2, 373. http://dx.doi.org/10.4236/ars.2013.24040.

Baath, G.S., Shukla, M.K., Bosland, P.W., Steiner, R.L., Walker, S.J., 2017. Irrigation water salinity influences at various growth stages of *Capsicum annuum*. Agric. Water Manage. 179, 246–253. http://dx.doi.org/10.1016/j.agwat.2016.05.028.

Backlund, V.L., Hoppes, R.R., 1984. Status of soil salinity in California. Calif Agric. 38 (10), 8–9.

BOSTID (Board on Science and Technology for International Development), 1990. Saline Agriculture Salt-tolerant Plants for Developing Countries. National Academy Press, Washington, DC, USA.

Chen, D., Huang, J., Jackson, T.J., 2005. Vegetation water content estimation for corn and soybeans using spectral indices derived from MODIS near-and short-wave infrared bands. Remote Sens. Environ. 98 (2), 225–236. http://dx.doi.org/10.1016/j.rse.2005.07.008.

Elnaggar, A.A., Noller, J.S., 2009. Application of remote-sensing data and decision-tree analysis to mapping salt-affected soils over large areas. Remote Sens. 2 (1), 151–165. http://dx.doi.org/10.3390/rs2010151.

FAO ITPS (2015). Status of the World's Soil Resources (SWSR). Main Report, Food and Agriculture Organization of the United Nations and Intergovernmental Technical Panel on Soils, Rome, Italy.

Fry, J.A., Xian, G., Jin, S., Dewitz, J.A., Homer, C.G., Limin, Y., Barnes, C.A., Herold, N.D., Wickham, J.D., 2011. Completion of the 2006 national land cover database for the conterminous United States. Photogramm. Eng. Rem. S 77 (9), 858–864.

Gao, F., Masek, J., Schwaller, M., Hall, F., 2006. On the blending of the landsat and MODIS surface reflectance: predicting daily Landsat surface reflectance. IEEE T Geosci. Remote. 44 (8), 2207–2218. http://dx.doi.org/10.1109/TGRS.2006.872081.

Gausman, H.W., Allen, W.A., 1973. Optical parameters of leaves of 30 plant species. Plant Physiol. 52 (1), 57–62. http://dx.doi.org/10.1104/pp.52.1.57.

Ghassemi, F., Jakeman, A.J., Nix, H.A., 1995. Salinisation of Land and Water Resources: Human Causes, Extent, Management and Case Studies. CAB International, Wallingford, Oxon, UK.

Gorji, T., Sertel, E., Tanik, A., 2017. Monitoring soil salinity via remote sensing technology under data scarce conditions: a case study from Turkey. Ecol. Indic. 74, 384–391. http://dx.doi.org/10.1016/j.ecolind.2016.11.043.

Hadjimitsis, D.G., Papadavid, G., Agapiou, A., Themistocleous, K., Hadjimitsis, M.G., Retalis, A., Michaelides, S., Chrysoulakis, N., Toulios, L., Clayton, C.R.I., 2010. Atmospheric correction for satellite remotely sensed data intended for agricultural applications: impact on vegetation indices. Nat. Hazards Earth Syst. Sci. 10, 89–95. http://dx.doi.org/10.5194/nhess-10-89-2010.

Han, W., Yang, Z., Di, L., Mueller, R., 2012. CropScape: a Web service based application for exploring and disseminating US conterminous geospatial cropland data products for decision support. Comput. Electron. Agric. 84, 111–123. http://dx.doi.org/10.1016/j.compag.2012.03.005.

R. Howitt, J. Medellín-Azuara, D. MacEwan, J. Lund, D. Sumner Economic Analysis of the 2014 Drought for California Agriculture, 2014, UC–Davis Center for Watershed Sciences Davis, CA, Available at: https://watershed.ucdavis.edu/files/biblio/DroughtReport_23July2014_0.pdf.

Huete, A., Jackson, R., Post, D., 1985. Spectral response of a plant canopy with different soil backgrounds. Remote Sens. Environ. 17 (1), 37–53. http://dx.doi.org/10.1016/0034-4257(85)90111-7.

Huete, A., Didan, K., Miura, T., Rodriguez, E.P., Gao, X., Ferreira, L.G., 2002. Overview of

the radiometric and biophysical performance of the MODIS vegetation indices. Remote Sens. Environ. 83 (1), 195–213. http://dx.doi.org/10.1016/S0034-4257(02)00096-2.
Ivits, E., Cherlet, M., Tóth, T., Lewińska, K., Tóth, G., 2011. Characterisation of productivity limitation of salt-affected lands in different climatic regions of Europe using remote sensing derived productivity indicators. Land Degrad. Dev. 24, 438–452. http://dx.doi.org/10.1002/ldr.1140.
Ivushkin, K., Bartholomeus, H., Bregt, A.K., Pulatov, A., 2017. Satellite thermography for soil salinity assessment of cropped areas in Uzbekistan. Land Degrad. Dev. 28 (3), 870–877. http://dx.doi.org/10.1002/ldr.2670.
Jönsson, P., Eklundh, L., 2004. TIMESAT—a program for analyzing time-series of satellite sensor data. Comput. Geosci. 30 (8), 833–845. http://dx.doi.org/10.1016/j.cageo.2004.05.006.
Kim, S., Prasad, A.K., El-Askary, H., Lee, W., Kwak, D., Lee, S., Kafatos, M., 2014. Application of the Savitzky-Golay filter to land cover classification using temporal MODIS vegetation indices. Photogramm. Eng. Rem. Sens. 80 (7), 675–685. http://dx.doi.org/10.14358/PERS.80.7.675.
Lambert, J.J., Southard, R.J., 1992. Distribution of Saline and Alkaline Soils in the San Joaquin Valley. A Map of Valley Soils. University of California Division of Agriculture and Natural Resources. Publication 21511. Oakland, CA, USA.
Lesch, S.M., Rhoades, J.D., Lund, L.J., Corwin, D.L., 1992. Mapping soil salinity using calibrated electromagnetic measurements. Soil Sci. Soc. Am. J. 56 (2), 540–548.
Letey, J., 2000. Soil salinity poses challenges for sustainable agriculture and wildlife. Calif. Agric. 54 (2), 43–48. http://dx.doi.org/10.3733/ca.v054n02p43.
Li, H., Lascano, R.J., Barnes, E.M., Booker, J., Wilson, L.T., Bronson, K.F., Segarra, E., 2001. Multispectral reflectance of cotton related to plant growth, soil water and texture, and site elevation. Agron. J. 93 (6), 1327–1337. http://dx.doi.org/10.2134/agronj2001.1327.
Liu, M., Wang, T., Skidmore, A.K., Liu, X., 2018. Heavy metal-induced stress in rice crops detected using multi-temporal Sentinel-2 satellite images. Sci. Total Environ. 637–638, 18–29.
Lobell, D.B., Ortiz-Monasterio, J.I., Gurrola, F.C., Valenzuela, L., 2007. Identification of saline soils with multiyear remote sensing of crop yields. Soil Sci. Soc. Am. J. 71 (3), 777–783. http://dx.doi.org/10.2136/sssaj2006.0306.
Lobell, D.B., Lesch, S.M., Corwin, D.L., Ulmer, M.G., Anderson, K.A., Potts, D.J., Doolittle, J.A., Matos, M.R., Baltes, M.J., 2010. Regional-scale assessment of soil salinity in the Red River Valley using multi-year MODIS EVI and NDVI. J. Environ. Qual. 39 (1), 35–41. http://dx.doi.org/10.2134/jeq2009.0140.
Maas, E., Hoffman, G., 1977. Crop salt tolerance\-current assessment. J. Irr. Drain Div. 103 (2), 115–134.
Maas, E., Poss, J., Hoffman, G., 1986. Salinity sensitivity of sorghum at three growth stages. Irrig. Sci. 7 (1), 1–11. http://dx.doi.org/10.1007/BF00255690.
McCabe, M.F., Wood, E.F., 2006. Scale influences on the remote estimation of evapotranspiration using multiple satellite sensors. Remote Sens. Environ. 105 (4), 271–285. http://dx.doi.org/10.1016/j.rse.2006.07.006.
Metternicht, G., Zinck, J., 2003. Remote sensing of soil salinity: potentials and constraints. Remote Sens. Environ. 85 (1), 1–20. http://dx.doi.org/10.1016/S0034-4257(02)00188-8.
Pettorelli, N., Vik, J.O., Mysterud, A., Gaillard, J.-M., Tucker, C.J., Stenseth, N.C., 2005. Using the satellite-derived NDVI to assess ecological responses to environmental change. Trends Ecol. Evol. 20, 503–510. http://dx.doi.org/10.1016/j.tree.2005.05.011.
Platonov, A., Noble, A., Kuziev, R., 2013. Soil salinity mapping using multi-temporal satellite images in agricultural fields of Syrdarya province of Uzbekistan. In: Shahid, S.A. (Ed.), Developments in Soil Salinity Assessment and Reclamation: Innovative Thinking and use of Marginal Soil and Water Resources in Irrigated Agriculture. Springer Science + Business Media Dordrecht, Dordrecht, the Netherlands, pp. 87–98.
R Core Team, 2017. R: A Language and Environment for Statistical Computing. R Foundation for Statistical Computing, Vienna, Austria.
Rouse J, Haas R, Schell J, Deering D, editors. 1973. Monitoring vegetation systems in the Great Plains with ERTS. Third ERTS symposium: NASA SP-351. pp. 309–317.
Savitzky, A., Golay, M.J., 1964. Smoothing and differentiation of data by simplified least squares procedures. Anal. Chem. 36 (8), 1627–1639. http://dx.doi.org/10.1021/ac60214a047.
Scudiero, E., Skaggs, T.H., Corwin, D.L., 2014a. Regional scale soil salinity evaluation using landsat 7, western san joaquin valley, California USA. Geoderma Reg. 2–3, 82–90. http://dx.doi.org/10.1016/j.geodrs.2014.10.004.
Scudiero, E., Teatini, P., Corwin, D.L., Ferro, N.D., Simonetti, G., Morari, F., 2014b. Spatiotemporal response of maize yield to edaphic and meteorological conditions in a saline farmland. Agron. J. 106, 2163–2174. http://dx.doi.org/10.2134/agronj14.0102.
Scudiero, E., Skaggs, T.H., Corwin, D.L., 2016b. Comparative regional-scale soil salinity assessment with near-ground apparent electrical conductivity and remote sensing canopy reflectance. Ecol. Indic. 70, 276–284. http://dx.doi.org/10.1016/j.ecolind.2016.06.015.
Scudiero, E., Corwin, D.L., Anderson, R.G., Skaggs, T.H., 2016a. Moving forward on remote sensing of soil salinity at regional scale. Front. Environ. Sci. 4, 65. http://dx.doi.org/10.3389/fenvs.2016.00065.
Scudiero, E., Corwin, D., Anderson, R., Yemoto, K., Clary, W., Wang, Z., Skaggs, T., 2017. Remote sensing is a viable tool for mapping soil salinity in agricultural lands. Calif Agr. 71, 231–238. http://dx.doi.org/10.3733/ca.2017a0009.
Solari, F., Shanahan, J., Ferguson, R., Schepers, J., Gitelson, A., 2008. Active sensor reflectance measurements of corn nitrogen status and yield potential. Agron. J. 100 (3), 571–579. http://dx.doi.org/10.2134/agronj2007.0244.
Tagarakis, A.C., Ketterings, Q.M., 2017. In-season estimation of corn yield potential using proximal sensing. Agron. J. 109, 1323–1330. http://dx.doi.org/10.2134/agronj2016.12.0732.
U.S. Salinity Laboratory Staff, 1954. USDA Handbook No. 60. In: Richards, L.A. (Ed.), Diagnosis and Improvement of Saline and Alkali Soils. U.S. Government Printing Office, Washington, D.C., USA.
Vermeulen, D., Van Niekerk, A., 2017. Machine learning performance for predicting soil salinity using different combinations of geomorphometric covariates. Geoderma 299, 1–12 j.geoderma.2017.03.013.
Vermote E. 2015. MOD09A1MODIS/Terra Surface Reflectance 8-Day L3 Global 500m SIN Grid V006. NASA EOSDIS Land Processes DAAC: https://doi.org/10.5067/modis/mod09a1.006.
Welle, P., Mauter, M., 2017. High-resolution model for estimating the economic and policy implications of agricultural soil salinization in California. Environ. Res. Lett. 12, 094010. http://dx.doi.org/10.1088/1748-9326/aa848e.
Williams, A.P., Seager, R., Abatzoglou, J.T., Cook, B.I., Smerdon, J.E., Cook, E.R., 2015. Contribution of anthropogenic warming to California drought during 2012–2014. Geophys. Res. Lett. 42 (16), 6819–6828. http://dx.doi.org/10.1002/2015GL064924.
Wu, W., Al-Shafie, W., Mhaimeed, A., Ziadat, F., Nangia, V., Payne, W., 2014. Soil salinity mapping by multiscale remote sensing in mesopotamia, Iraq. . IEEE J. Sel. Top. Appl. 7, 4442–4452. http://dx.doi.org/10.1109/jstars.2014.2360411.
Xiao, X., Boles, S., Liu, J., Zhuang, D., Frolking, S., Li, C., Salas, W., Moore, B., 2005. Mapping paddy rice agriculture in southern China using multi-temporal MODIS images. Remote Sens. Environ. 95 (4), 480–492. http://dx.doi.org/10.1016/j.rse.2004.12.009.
Zare, E., Huang, J., Santos, F., Triantafilis, J., 2015. Mapping salinity in three dimensions using a DUALEM-421 and electromagnetic inversion software. Soil Sci. Soc. Am. J. 79 (6), 1729–1740. http://dx.doi.org/10.2136/sssaj2015.06.0238.
Zhang, T., Zeng, S., Gao, Y., Ouyang, Z., Li, B., Fang, C., Zhao, B., 2011. Using hyperspectral vegetation indices as a proxy to monitor soil salinity. Ecol. Indic. 11 (6), 1552–1562. http://dx.doi.org/10.1016/j.ecolind.2011.03.025.
Zhang, T., Qi, J., Gao, Y., Ouyang, Z., Zeng, S., Zhao, B., 2015. Detecting soil salinity with MODIS time series VI data. Ecol. Indic. 52, 480–489. http://dx.doi.org/10.1016/j.ecolind.2015.01.004.
Zhu, L., Radeloff, V.C., Ives, A.R., 2017. Improving the mapping of crop types in the Midwestern US by fusing Landsat and MODIS satellite data. Int. J. Appl. Earth Obs. 58, 1–11. http://dx.doi.org/10.1016/j.jag.2017.01.012.